The Structure of the Wind-Driven Circulation in the Subtropical South Pacific Ocean*

RUI XIN HUANG

Department of Physical Oceanography, Woods Hole Oceanographic Institution, Woods Hole, Massachusetts

BO QIU

Department of Oceanography, University of Hawaii at Manoa, Honolulu, Hawaii

(Manuscript received 12 March 1996, in final form 18 September 1997)

ABSTRACT

The structure of the wind-driven circulation in the subtropical South Pacific is studied using simple diagnostic and analytical models. The diagnostic calculation is based on the Levitus climatology. The analytical model is forced by observed winter mixed layer density and depth calculated from the Levitus climatology and by the surface wind stress data from the Hellerman and Rosenstein climatology. The wind-driven gyre in the South Pacific is relatively deep, reaching 2.4 km along the southern edge of the gyre. The gross feature of subduction obtained from both the data analysis and the analytical model is similar, with an annual ventilation rate of 21.6 Sv (Sv $\equiv 10^6$ m^3 s^{-1}), including 18.1 Sv from vertical pumping and 3.5 Sv from lateral induction. Although the annual subduction rate in the South Pacific is comparable to that in the North Atlantic, lack of localized subduction leads to relatively weak mode water formation in the region where the East Australian Current separates from its western boundary. In addition, results from the analytical model indicate the existence of an isopycnal slope reversal in the southeastern Pacific.

1. Introduction

Motion in the upper kilometer of the ocean is primarily wind driven. The horizontal and vertical motion in this layer plays a significant role in controlling the interaction between the atmosphere and the ocean. The structure of the wind-driven circulation is consequently of vital importance to our understanding of the oceanic general circulation and climate.

In the 1980s, theories about the baroclinic structure of the wind-driven gyre advanced rapidly. Rhines and Young (1982a,b) proposed the idea of potential vorticity homogenization and applied it to the deeper part of the wind-driven circulation, the unventilated thermocline. A multilayer model for the ventilated thermocline was put forth by Luyten et al. (1983, hereafter LPS). For simplicity, the mixed layer was neglected in the original multilayer model of the ventilated thermocline. The dynamic role of the mixed layer in the ventilation/subduction process was emphasized by Woods (1985). Most

importantly, Woods showed that a horizontal gradient of mixed layer depth can substantially enhance the subduction rate. This enhancement has been demonstrated by Sarmiento (1983) and Jenkins (1982, 1987) through tracer observations within the thermocline.

An added complication is the seasonal cycle in the upper ocean. Although Iselin (1939) found a connection between winter conditions at the sea surface and water mass characteristics in the permanent thermocline below, he had no dynamical theory to explain their relationship. Stommel (1979) presented a simple and elegant view of the time-dependent subduction process, now called the ''Stommel demon.'' The mixed layer's density and depth reach their local maxima during late winter. Since the mixed layer rapidly retreats in early spring, water subducted into the permanent thermocline has properties that are strongly biased toward the late winter values.

More recently, the LPS model has been extended to a continuously stratified ocean (Huang 1988, 1990). The model is forced by climatological mixed layer density and depth fields. Since the model is based on the assumption of a climatological-mean steady circulation, it cannot directly apply to cases in which the mixed layer undergoes seasonal variations. However, if one is interested in only the annual-mean mass fluxes (or the subduction rate), the details of the seasonal cycle may not be so important and we may estimate this rate without involving the seasonal cycle explicitly. For details,

---

Corresponding author address: Dr. Rui Xin Huang, Department of Physical Oceanography, Woods Hole Oceanographic Institution, Woods Hole, MA 02543.
E-mail: huang@dragon.whoi.edu

the reader is referred to a recent study by Qiu and Huang (1995) in which different definitions of the subduction rates and their relationships were compared and a comprehensive review of this subject was provided.

The multilayer ventilated thermocline model was initially applied to the North Atlantic by LPS with great success. Talley (1985) subsequently applied the model to the North Pacific and replicated many of the observed features in the ventilated thermocline. De Szoeke (1987) applied the LPS model to the subtropical South Pacific and showed that the distribution of the Sverdrup transport among density layers in the upper ocean can be successfully explained by the ventilated thermocline theory.

In order to improve our understanding of the structure of wind-driven circulation, more elaborate models have been applied to the oceans. Using an analytical model that includes the observed mixed layer depth and horizontal density gradient, Huang (1990) determined the three-dimensional structure in the ventilated and unventilated thermocline of the North Atlantic. Focusing on the mass transfer from the mixed layer to the thermocline, Marshall et al. (1993) estimated the subduction rate and period of effective detrainment in the North Atlantic based on the Levitus (1982) temperature/salinity and Isemer and Hasse (1987) wind datasets. Over the major part of the subtropical North Atlantic, they found that effective detrainment, which contributes to subduction, takes place over a short time period, about 1 to 2 months, in late winter/early spring. This short time span of effective detrainment is further confirmed in a recent numerical study by Williams et al. (1995).

Subduction of the winter mixed layer water and the three-dimensional structure of the wind-driven circulation in the North Pacific was studied by Huang and Qiu (1994) using a diagnostic approach, and by Huang and Russell (1994) using a continuously stratified North Pacific model. In these two studies, the authors emphasized the difference in the thermohaline circulation between the North Pacific and the North Atlantic and the resultant effect on the two oceans' thermocline ventilation.

The oceanic circulation in the Southern Hemisphere is different from that in the Northern Hemisphere in several respects. Because of different landmass distributions, the atmospheric forcing of the respective oceans is considerably different. For example, stronger Ekman pumping (due to stronger wind stress curl) over the Northern Hemisphere oceans results in more intense western boundary currents, which transport a greater amount of heat meridionally. This heat transport influences air–sea buoyancy fluxes at midlatitudes and has a great impact on the regional ventilation processes. The presence of the Antarctic Circumpolar Current (ACC) in the Southern Ocean complicates the general circulation and water mass formation in the Southern Hemisphere oceans.

The objective of the present study is to clarify the

baroclinic structure of the wind-driven circulation in the South Pacific Ocean. The large-scale circulation of this ocean has been previously documented by Reid (1965, 1986), Warren (1973), and de Szoeke (1987). While de Szoeke's study highlighted the main features of the wind-driven circulation in the South Pacific, some important aspects of the dynamics, involving the mixed layer and the unventilated thermocline, were omitted.

We will focus on the baroclinic structures of the wind-driven circulation in the subtropical South Pacific, including the mixed layer and the unventilated thermocline. A diagnostic approach utilizing available climatological datasets will be discussed in section 2, including the subduction rate map and the overall vertical structure of the wind-driven circulation. An analytical model using an idealized South Pacific Ocean with continuous stratification will be described in section 3, including the detailed structure of the South Pacific subtropical gyre. In section 4, we will summarize the results from this study.

2. The diagnostic calculation

Our diagnostic calculations are based on the Stommel (1979) demon hypothesis wherein water masses subducted into the permanent pycnocline have late winter properties. A crucial assumption here is that the retreat of the winter mixed layer, or the formation of the seasonal pycnocline, takes place in a relatively short time period. As in the subtropical North Atlantic and North Pacific, this condition is met satisfactorily in the subtropical South Pacific. Maps of the monthly mixed layer depth calculated from Levitus (1994) data indicate that the mixed layer in the subtropical South Pacific reaches its annual maximum in September and retreats to shallow depth in a period of less than 2 months.

The South Pacific mixed layer depth and density in September show in addition to poleward trends a strong, east–west asymmetry (Fig. 1). The mixed layer depth exceeds 150 m in the eastern part of the subtropical basin, whereas it is less than 50 m in the northwest corner of the basin. Unlike the situation in the North Pacific, continental influence over the South Pacific is weak. The winter maximum surface heat flux from the ocean to the atmosphere above the East Australian Current is less than 150 W m^{-2} (Oberhuber 1988). This is in great contrast to the North Pacific where the winter maximum surface heat flux over the Kuroshio Extension region can exceed 350 W m^{-2}. Reduced cooling due to the absence of continental cold, dry polar air results in relatively shallow and spatially uniform mixed layers near the western boundary of the subtropical South Pacific. As will be discussed later, this leads to a small lateral induction rate in the western boundary outflow region, and a small subduction rate there.

A sharp transition in winter mixed layer thickness exists across the South Pacific Subtropical Front (about 45°S), which is closely related to subantarctic mode

a) Mixed layer depth (m) in September
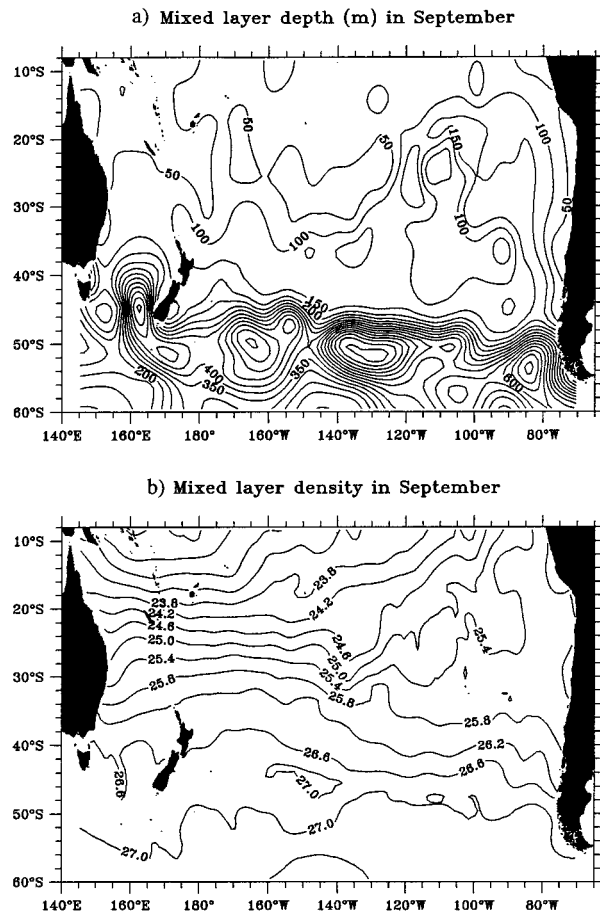

b) Mixed layer density in September

FIG. 1. September mixed layer depth (a) and density (b) of the South Pacific Ocean. Here mixed layer depth is defined as the depth at which σ_θ is 0.125 greater than the surface σ_θ. Calculated from Levitus (1994) monthly climatology.

water formation (McCartney 1977). The winter mixed layer depth in the South Pacific subpolar region is, in general, much greater than in the subpolar North Pacific, see Fig. 1 in Huang and Qiu (1994). This difference in mixed layer depth reflects the remarkable difference in vertical stratification in these two basins.

Since precipitation exceeds evaporation in the subpolar North Pacific, a shallow halocline develops that restricts the winter convection to a relatively shallow layer. On the other hand, due to the influence from both the Atlantic and Indian Oceans, salinity in the ACC is high (34–35 psu). The strong westerly over the ACC induces strong vertical mixing and creates a relatively weak stratification both in the ACC and near the subantarctic front (both temperature and salinity gradients are weak). As a result, winter cooling can penetrate much deeper.

The density distribution of the winter mixed layer in the South Pacific is clearly oriented zonally (Fig. 1b). The exception appears in the southeast and north of the ACC where low-salinity water is formed by the exces-

sive precipitation and creates a shallow halocline. Since this low-salinity water is relatively light, it gives rise to a slight SE–NW orientation of the isopycnals. In contrast, evaporation dominates in the North Atlantic, and isopycnals have a NE–SW orientation in the eastern subtropics. The maximum mixed layer density in the South Pacific involved in the wind-driven ventilation is about $27.4\sigma_\theta$ (see Fig. 1b), which falls in between the maximum density values of the North Pacific ($26.6\sigma_\theta$) and the North Atlantic ($27.7\sigma_\theta$).

To estimate the annual mean subduction rate (S_{ann}) in the South Pacific, we traced particles released at the base of the winter mixed layer and used the definition in Lagrangian coordinates:

$$S_{\text{ann}} = -\overline{\left(w_{\text{Ek}} - \frac{\beta}{f} \int_{-h_m}^{0} v_m \, dz \right)} + \overline{\mathbf{u}_m \cdot \boldsymbol{\nabla} h_m}, \quad (1)$$

where the subscript m indicates the quantities for the mixed layer and the term in parentheses on the right-hand side denotes the contribution from vertical pumping; the second term is from lateral induction. In the vertical pumping term, w_{Ek} is the Ekman pumping velocity and the β term gives a correction to the vertical pumping velocity (at the base of the mixed layer) due to the meridional velocity. The overbar indicates an average over the 1-yr trajectory. In Lagrangian coordinates, the lateral induction term $\overline{\mathbf{u}_m \cdot \boldsymbol{\nabla} h_m}$ is simply the difference of the mixed layer depth at particle positions separated in time by one year, $h_{m,0} - h_{m,1}$. Qiu and Huang (1995) recently compared various definitions for S_{ann} and discussed their differences; the reader is referred to their section 2 for details.

To obtain the velocities along isopycnal surfaces on which particle trajectories are traced, we calculated the acceleration potential values from the annual Levitus (1994) dataset and converted them to isopycnal velocities assuming a zero-velocity surface at 2000-m depth (Fig. 2). This reference level had been previously used by Warren (1973) in his study of the deep circulation in the South Pacific. One reason for choosing this level was that it lies in the middle of the deep oxygen minimum layer, which can be interpreted as a layer of very small horizontal velocity (Warren 1973). Although recent studies indicate that this oxygen minimum layer moves southward (Toole et al. 1994), choosing slightly different zero-velocity surfaces, such as 2500 m, gives almost the same subduction rate.

The annual-mean Ekman pumping velocity in Eq. (1) is calculated from the Hellerman and Rosenstein (1983, hereafter HR) wind stress data. There has been concern expressed about the drag coefficient used in the HR calculation. As pointed out by Harrison (1989) and Trenberth et al. (1990), the HR wind stress data are about 20% higher than the result based on a more accurate bulk formula by Large and Pond (1981). This conclusion was also reached by Chelton et al. (1990) in their study of the global wind stress using the Seasat scatterometer
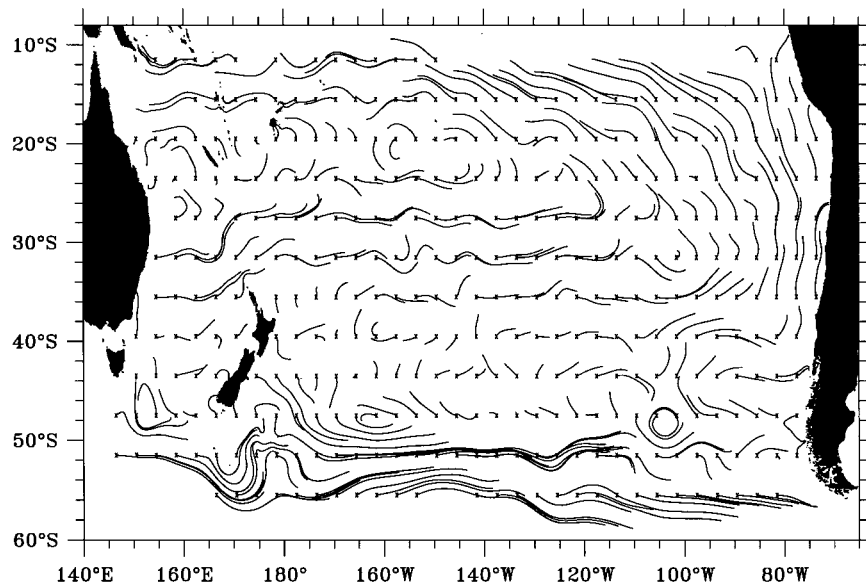
FIG. 2. Lagrangian trajectories over a 1-yr period. The starting points are indicated by crosses where the particles are released from the base of the mixed layer in September.

data. Following these studies, we used the HR wind stress data in this study with their magnitude reduced by 20%. The maximum streamfunction value calculated using these reduced HR data is 36 Sv (Sv $\equiv 10^6$ m^3 s^{-1}), Fig. 3.

a. Subduction

As we noted in Eq. (1), the annual-mean subduction rate consists of two terms: the vertical pumping term at the base of the winter mixed layer and the lateral induction term due to slope of the mixed layer base. The vertical pumping value is generally smaller than that of the Ekman pumping due to meridional motion in the mixed layer. In the subtropical South Pacific, however, this difference is small (cf. Figs. 4a and 4b) because the
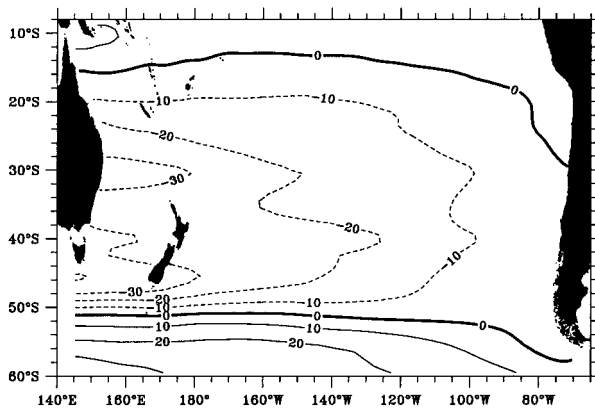

FIG. 3. Sverdrup transport streamfunction calculated using the (reduced by 20%) annual surface wind stress climatology by Hellerman and Rosenstein (1983).

winter mixed layer in most regions is no more than 100 m.

Because of the horizontal changes in depth of the winter mixed layer, water can either leave or enter the mixed layer from the permanent pycnocline. In the subtropical South Pacific, the mixed layer depth increases slightly from west to east. Since there is no local mixed layer depth maximum near the western boundary current separation latitude, no strong lateral induction occurs there (Fig. 4c). This is in sharp contrast to both the North Pacific and the North Atlantic, where strong mixed layer depth gradients in the western boundary outflow regions cause a large lateral induction from the mixed layer to the permanent pycnocline.

The estimated lateral induction rate in the South Pacific is quite noisy with regionally alternating sign. Regions of large, positive and negative values appear primarily along the edge of the ACC (Fig. 4c). The existence of such large features in the lateral induction rate is a direct result of the large disturbances in the mixed layer depth map (Fig. 1a) and is likely to be a reflection of the noisy nature of the mixed layer depth or the paucity of data in that area. The distribution of the subduction rate (Fig. 4d) also contains many large disturbances, a product of the noisy lateral induction rate.

b. Vertical structure

Using the results from the diagnostic calculation, we summarize the three-dimensional structure of the wind-driven gyre in the South Pacific in a four-layer model, Fig. 5. For a comparison between results from the diagnostic and analytical models, the subduction rate cal-
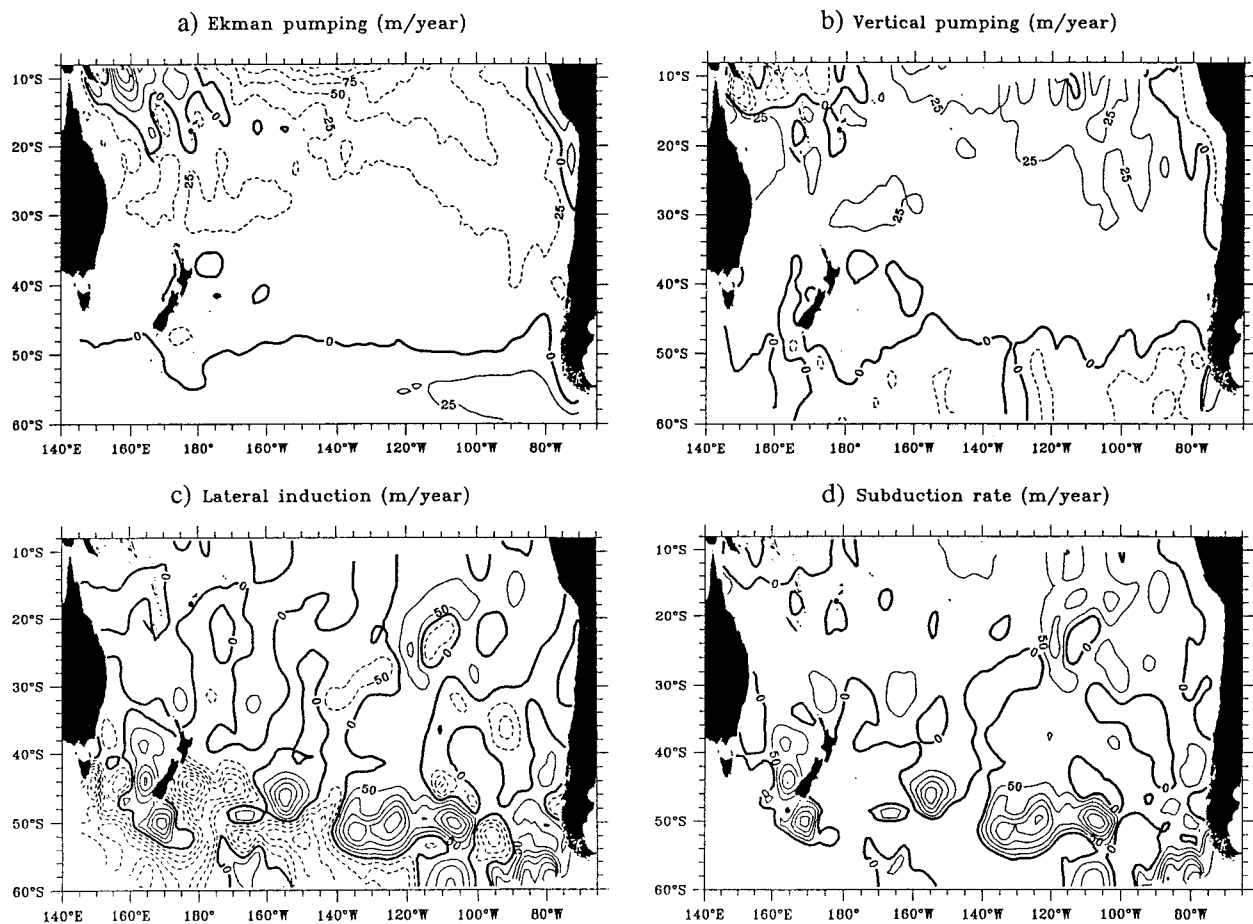
FIG. 4. Subduction rate maps from the diagnostic model: (a) Ekman pumping rate, (b) vertical pumping rate at the base of the mixed layer, (c) lateral induction rate at the base of the mixed layer, and (d) subduction rate.

culation here is for a region from 48°S to 16°S and from 160°E to the South American coast. The ocean is divided vertically into four layers: the Ekman layer on top, the mixed layer (or the seasonal thermocline), the ventilated thermocline, and the unventilated thermocline on the bottom.

In our diagnostic model the Ekman layer is treated as an infinitely thin layer, and its only function is to produce the Ekman pumping required for driving the geostrophic flow below. The geostrophic flux in the Ekman layer is regarded as a part of the geostrophic flow in the mixed layer below. There is 18.1 Sv of Ekman flux entering from the northern boundary, 7.2 Sv entering from the southern boundary, and 1.3 Sv is entering from the eastern boundary and leaving from the western boundary, producing a total amount of Ekman pumping of 25.3 Sv.

Below the Ekman layer lies the mixed layer, or the seasonal thermocline, whose lower boundary is defined as the annual mixed layer depth maximum. The base of the seasonal thermocline is slightly slanted, reflecting the general feature of the September mixed layer depth map in Fig. 1a. Ekman pumping from the top results in

a generally northward geostrophic motion. As a result, there is a mass flux of 0.9 Sv entering the southern boundary and 11.6 Sv leaving the northern boundary. In addition, the counterclockwise geostrophic circulation induces a mass flux of 6.2 Sv from the southern part of the western boundary (from 48°S to 25°S). The mass exchange rate between the seasonal thermocline and the ventilated thermocline is 21.6 Sv, including 18.1 Sv from vertical pumping [the first term in (1)] at the base of the mixed layer and 3.5 Sv from lateral induction [second term in (1)].

The ventilated thermocline in this simple four-layer system is defined as between the annual mixed layer depth maximum and the $\sigma_\theta = 27.0$ isopycnal surface. The 21.6 Sv of mass flux from subduction enters the ventilated thermocline and moves out through the northern and western boundaries. There is a mass flux of 6.4 Sv entering this layer from the southern part of the western boundary, 2.3 Sv from the southern boundary, and 3.6 Sv from the eastern boundary. (Strictly speaking, these mass fluxes should be classified as part of the unventilated thermocline because they do not come from the mixed layer.) Note that the directions of these mass
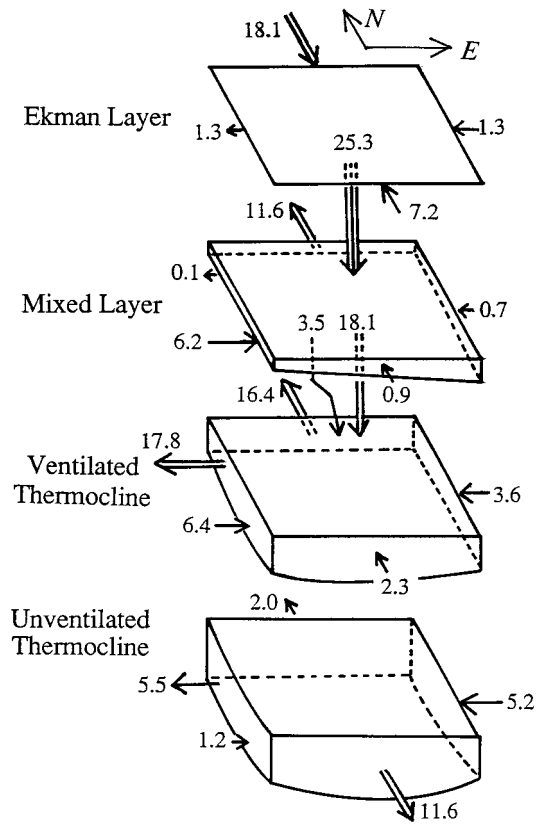
FIG. 5. Mass flux (in Sverdrups) partition in the wind-driven subtropical gyre of the South Pacific (48°–16°S, 160°E–South American coast) from the diagnostic model. The transport values for the Ekman layer are based on the HR climatological wind data. The transport values through the lateral boundaries of the thermocline layers are estimated from the geostrophic flows with a reference at 2000 m.

fluxes agree well with the flow directions derived by Reid (1986, his Fig. 7) on the isopycnal surface $\sigma_\theta = 26.4$.

The unventilated thermocline is defined as below the $\sigma_\theta = 27.0$ isopycnal surface. Mass fluxes in this layer are calculated from the geostrophic velocity relative to the 2000-m reference level (between $\sigma_\theta = 27.0$ and 2000 m). It is assumed that there is no mass exchange across the upper and lower surfaces of the unventilated thermocline. The lateral mass fluxes in this layer do not balance; in fact, there is a net loss of 12.7 Sv. There are two possible reasons for this imbalance. First, the 2000-m depth may not be a suitable reference level. Although appropriate for the eastern part of the South Pacific along 32°S, Toole et al. (1994) recently argued that bottom velocity is southward on the western flank of the East Pacific Rise, so the reference level should be placed at the bottom of the ocean. Because of the coarse vertical resolution of the Levitus data below 2000 m, the issue of using variable reference depths is not addressed in this study. The existence of thermohaline overturning cells in the South Pacific, which is neglected in this study of the wind-driven circulation, is another

likely contributor to the mass flux imbalance in the unventilated thermocline. The influence of the thermohaline circulation upon the unventilated thermocline mass balance is beyond the scope of this study and is left for future studies.

3. The analytical model

Our analytical approach is to solve a free-boundary value problem in the density coordinates described by Huang (1990) and Huang and Russell (1994). Accordingly, the wind-driven circulation, including the density and velocity structure in the upper ocean, can be calculated by repeatedly solving an ordinary differential equation at each station in a subtropical basin. The model treats the wind-driven circulation as a perturbation to a specified background stratification for the abyssal waters and the potential vorticity for the unventilated thermocline. As demonstrated by Huang (1990) and Huang and Russell (1994), the calculation of the ideal-fluid thermocline is reduced to repeatedly solving the following free boundary value problem in density coordinates:

$$B_{\rho\rho} = \frac{fg}{Q(B, \rho)} \qquad (2)$$

with the constraints

$$B_\rho = gh(x, y) \qquad \text{at } \rho = \rho^s \qquad (3)$$

$$B = B^a(\rho), \qquad B_\rho = B^a_\rho(\rho) \quad \text{at } \rho = \rho^b$$
$$(\rho^b \text{ is unknown}) \qquad (4)$$

$$-\int_{\rho^s}^{\rho^b} B_\rho^2 \, d\rho + \int_{\rho^{be}}^{\rho^b} B^{a2}_\rho \, d\rho = \frac{2g\bar{\rho}f^2}{\beta} \int_x^{x^e} w_e \, dx, \qquad (5)$$

where $B = p + \rho gz$ is the Bernoulli function; Q is the potential vorticity; $h(x, y)$ is the mixed layer depth, which is specified; g is the gravitational acceleration; w_e is the Ekman pumping rate; subscript ρ indicates partial derivative with respect to density; superscript s indicates the sea surface; superscript b indicates the base of moving water; and superscript a indicates abyss (below the moving water in the thermocline).

This free boundary value problem is solved using a shooting method by starting from a first guess at the bottom of the moving water ρ^b (the density at the bottom of the moving water in an adjacent station can be used as the first guess.) Integrating upward (toward lower density) to the base of the mixed layer, we can determine the potential vorticity of the uppermost ventilated layer as $q = f\Delta\rho/\Delta h$, where $\Delta\rho$ is the density increment and Δh is the thickness of the uppermost layer. The generalized Sverdrup relation is then checked. If it is not satisfied, the base of the moving water, ρ^b, is adjusted until the integral constraint is met.

As the zero line of Ekman pumping in the South Pacific closely follows the outcropping line of $\sigma_\theta = 27.0$, this isopycnal outcropping line is chosen as the

southern boundary of the model, and this isopycnal surface is used to separate the ventilated thermocline from the unventilated thermocline. For the ventilated thermocline, we divided each isopycnal outcropping line into 65 segments and applied our analytical method to the 16 isopycnal outcropping lines (starting from $\sigma_\theta = 27.0$ with an increment of $-0.2\sigma_\theta$). Notice that the isopycnal outcropping lines in the South Pacific Ocean have a fairly complex distribution (Fig. 1b). However, as long as there is no closed outcropping line, solving the boundary value problem as described above is straightforward.

a. Forcing the model with Levitus data

The model requires the background stratification to be specified for both the abyssal waters and the unventilated thermocline. The background stratification used in this study consists of two parts, so it is slightly different from that used by Huang and Russell (1994). The shallow part was obtained by averaging the mean density profiles at two sections in the equatorial Pacific, 120°W and 140°W in the Levitus climatology. Both of these density profiles were averaged between 15°N and 15°S. The deep part was obtained by averaging the stratification below the winter mixed layer along 100°W and between 15°S and 50°S. This is some distance from the eastern boundary, so the effect of the coastal upwelling on the stratification is minimized. The two profiles are matched smoothly over the density range $\sigma_\theta = 25.0$–25.4. Use of background stratification near the eastern boundary reflects that wind-driven circulation there is relatively shallow, the so-called shadow zone; thus, the stratification there can be used as the undisturbed background stratification set up by the thermohaline circulation.

Rhines and Young (1982a,b) showed that potential vorticity in the unventilated thermocline is homogenized toward its value along the poleward boundary. Their theory was extended to the circumpolar oceans by Haynes (1985), who showed that in the case of a zonal current, potential vorticity should be homogenized toward the planetary vorticity at the latitude of the boundary between the undisturbed zonal current and the ambient water. The northern edge of the circumpolar current is rather difficult to define in our model. We first smoothed the observed winter mixed-layer properties, Fig. 6 (cf. Fig. 1). As noted above, the outcropping line $\sigma_\theta = 27.0$ follows closely the zero-Ekman-pumping line, and is thus chosen as the southern boundary of our analytical model. Since this southern boundary is not along a constant latitude, we have chosen the eastern tip of the southern boundary along 54°S as the reference southern boundary, so the potential vorticity of the unventilated thermocline is assumed to be homogenized toward the value along this part of the southern boundary.

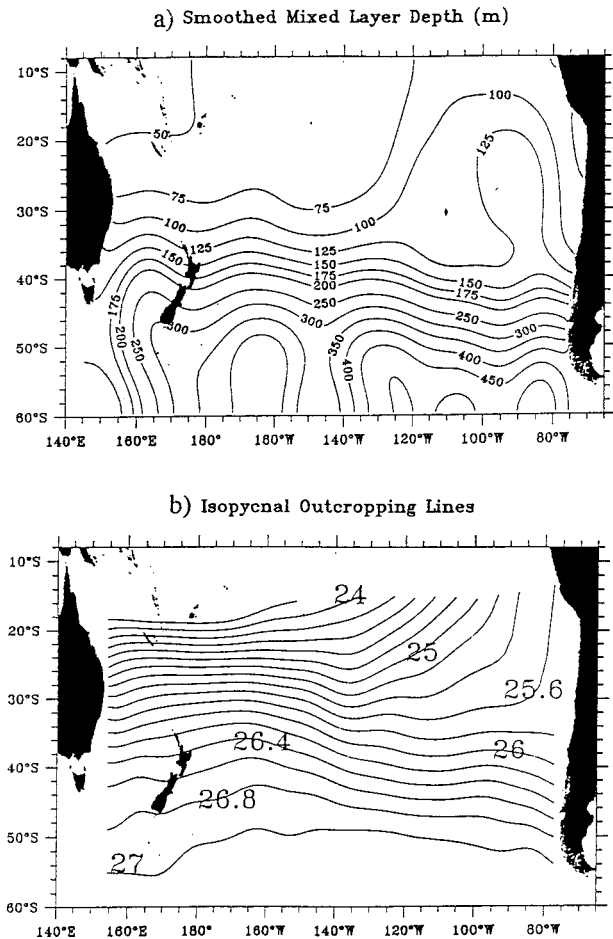The northern boundary consists of two parts. The

FIG. 6. Smoothed mixed layer depth (a) and density (b) fields used for the analytical model.

western section is along the isopycnal outcropping line $\sigma_\theta = 23.8$, and the eastern section is along 15°S. The eastern boundary is along 77.5°W and the western boundary is at 153°E. To facilitate the analytical calculation, all islands (such as New Zealand) and topographic features inside the model domain are ignored.

The model integration started from the isopycnal outcropping line of $\sigma_\theta = 26.8$ and moved northward line by line. Although the program converged satisfactorily for the first 14 outcropping lines, the model's convergence became poor for outcropping lines lighter than $24.4\sigma_\theta$. At some isolated stations, the program failed to provide an exact solution for Eq. (5). To remedy this problem, we seek solutions in these isolated stations that minimize the difference between the left-hand side and the right-hand side of the generalized Sverdrup relation [Eq. (5)]. Since these stations are isolated, they do not affect the global structure of the solution.

This problem is also reflected in the map of potential thickness for the uppermost layer (Fig. 7; here, potential thickness is defined as the inverse of potential vorticity). From this map, it is clear that the upper-layer thickness
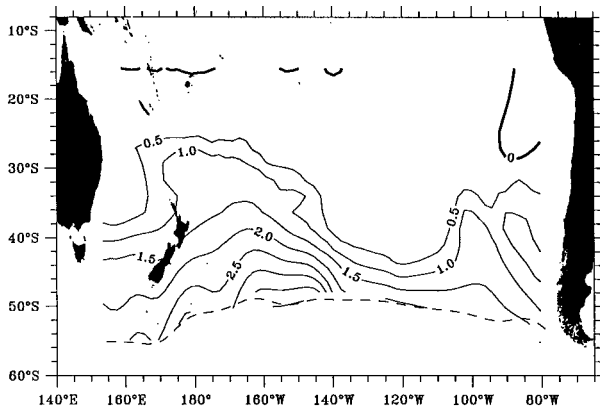
FIG. 7. Upper-layer potential thickness, in 10^{-9} σ cm^{-1} s^{-1}, determined from the analytical model. Here potential thickness is defined as the inverse of the potential vorticity.

FIG. 8. Sea surface topography (in cm) determined from the analytical model.

gets progressively thinner as one approaches the northern part of the basin. Apparently, layer thickness obtained from the analytical model becomes negative in the northeastern corner and along the northern boundary. A negative thickness for the ventilated thermocline is, of course, physically meaningless. Somehow, the model could not keep up with more and more moving layers with finite thicknesses and started to give negative thickness for the uppermost ventilated layer. The exact cause of such peculiar behavior of the continuously stratified model remains a mystery to us at this time. One possible explanation is that the Levitus (1994) data are inadequate in representing the climatology of the South Pacific Ocean. The negative layer thickness near the western coast of Peru may reflect that El Niño–Southern Oscillation activity is such a strong component of the oceanic circulation that the basic assumption of the so-called climatological-mean steady circulation is no longer valid here. Furthermore, the Levitus climatology may inadequately estimate the time-mean density fields. Nevertheless, the area of negative potential vorticity occupies only a very small part of the basin, so the global picture provided by our calculation may still be useful.

b. The sea surface topography

The Bernoulli function in the mixed layer calculated from the analytical model implies a sea surface elevation

$$\eta = \frac{B^s}{g\bar{\rho}}. \qquad (6)$$

Choosing a zero reference level at the southeast corner, we find that the sea surface in the South Pacific has a maximum elevation of 80 cm near the western boundary in the center of the subtropical gyre (Fig. 8). The sea surface topography suggests a generally eastward motion in the southern half of the subtropical basin and a northeastward motion in the northern half. In the middle
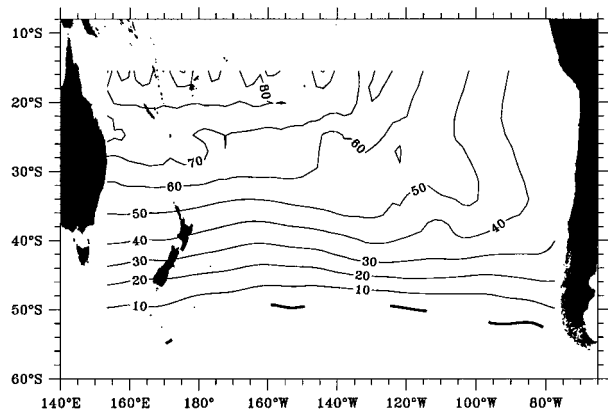
of the basin there seems to be the vague sign of a local maximum at 30°S between 150°W and 100°W.

The presence of the local maximum of sea surface height can also be seen in the slope of subsurface isopycnals. Along the 35°S section it is clear that the isopycnal slope reversal can reach as deep as 300 m east of 100°W (Fig. 9). The reversed isopycnal slope indicates $v_z < 0$; thus it implies a subsurface equatorward velocity maximum. In both cases, the surface motion relative to that below resembles an eastern gyre. M. M. Hall et al. (1989, unpublished manuscript) analyzed the 2–3-yr long current meter records at several stations along 152°W and found a subsurface equatorward velocity maximum at 100–200 m depth for a station at 35°N. The existence of an eastern gyre associated with this isopycnal slope reversal was discussed by Hautala et al. (1994). The isopycnal slope reversal and the associated subsurface meridional velocity maximum were reproduced in the analytical model of the wind-driven circulation in the North Pacific by Huang and Russell (1994).
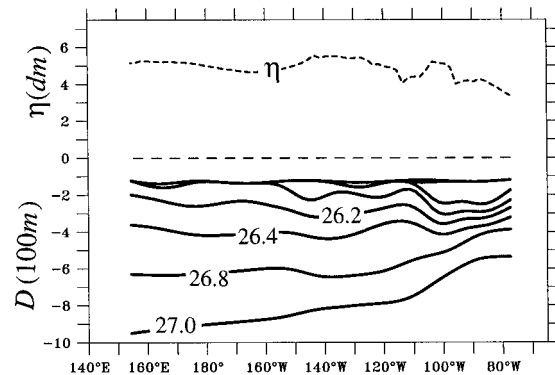
From a recent World Ocean Circulation Experiment

FIG. 9. A zonal section along 35°S from the analytical model. The short dashed line indicates the free surface elevation (exaggerated, in decimeters) and solid lines indicate isopycnals (in σ_θ). The long dashed line indicates the $z = 0$ level.

(WOCE) hydrographic section taken along 32°S, Toole et al. (1994) observed a clear isopycnal slope reversal in the upper 500 m in the eastern South Pacific. With a deep reference level, surface dynamic height has two local maxima at 155°E and 120°W, respectively, and a minimum near the dateline. The existence of the sea surface height maximum in the eastern basin is also confirmed in a recent study by C. J. Koblinsky et al. (1995, personal communication), in which they showed a local sea surface height maximum located east of 170°W in the South Pacific both from TOPEX altimeter data and from WOCE hydrographic data along 32°S. In comparison, the high-resolution numerical model shows a relatively narrower local maximum east of 140°W.

A similar map of sea surface topography relative to 2000 db was also generated from the Levitus (1994) data, and it has a global feature rather similar to the analytic result discussed above and the adjusted steric height map by Reid (1986). However, neither the map from the Levitus data nor Reid's map shows the local sea surface maximum discussed above. This is probably due to the shallow nature of this local surface height maximum.

c. The structure of the wind-driven gyre

In Welander's (1971) work on the ideal-fluid thermocline, the base of the moving water is assumed to have constant density ρ^∞. In the LPS model and de Szoeke's (1987) model each layer has its own shadow zone, which is separated into many small subzones according to the different functional relationship between the potential vorticity and the Bernoulli function. In our simple numerical approach, however, the shadow zones appear naturally as the stagnant abyssal water below the moving water (Fig. 10). In comparison with de Szoeke's (1987) solution, our present model provides a much more finely divided picture of the shadow zone. Consider, for example, the $\sigma_\theta = 27.3$ isopycnal. Water to the northeast of the line marked by 27.3 (Fig. 10a) is stagnant, comprising the shadow zone for this isopycnal.

The base of the wind-driven gyre is relatively deep in the subtropical South Pacific, having a maximum depth of about 2.4 km (Fig. 10b). This is considerably deeper than in the North Pacific [no more than 1.4 km, Huang and Russell (1994)] and in the North Atlantic [about 1.75 km, Huang (1990)]. Such a deep, wind-driven circulation in the South Pacific is associated with the large meridional gradient of winter mixed-layer depth along the southern edge of the subtropical gyre.

Our estimates of the wind-driven gyre in these oceans are based on the same analytical model; however, other models' estimates may be different. For example, the potential vorticity distribution in the North Pacific indicates that the wind-driven gyre may penetrate down to greater than 2000 m (e.g., Talley 1985, 1988) if one assumes that regions of potential vorticity homogeni-
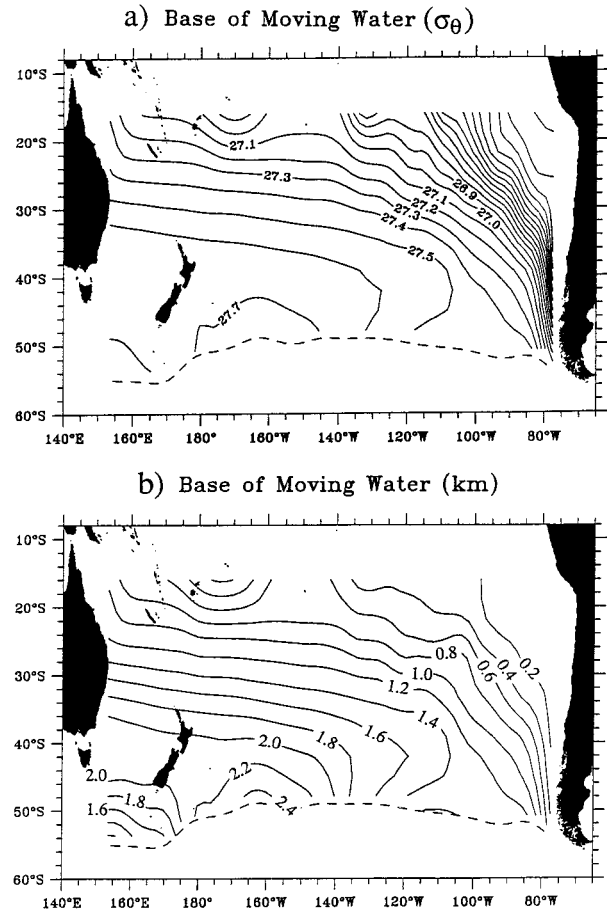

FIG. 10. Base of the moving water determined from the analytical model: (a) density in σ_θ and (b) depth in kilometers.

zation in the ocean interior are linked to the wind-driven circulation.

The three-dimensional structure of the wind-driven circulation can be seen from layer depth maps and streamline patterns (the Bernoulli function contours) on each isopycnal surface, such as in Figs. 11 and 12. At a shallow isopycnal surface, $\sigma_\theta = 26.2$, there is a very narrow shadow zone in the northeastern corner, not shown in Fig. 11. The streamline pattern indicates the passage of a water parcel after subduction along the southern edge where the isopycnal $\sigma_\theta = 26.2$ outcrops, as indicated by the dashed line. The shadow zone becomes much larger for the unventilated isopycnal surfaces, as shown in Fig. 12. Since this isopycnal is unventilated, all water in this layer comes out through the western boundary and returns through the western boundary entirely.

The subduction rate map calculated from our analytical model is consistent with that from the diagnostic model. Similar to the results shown in Fig. 4, large disturbances appear along the southern edge of the subtropical gyre, Fig. 13. If we calculate the subduction rate by adding both positive and negative values, we

a) Depth of σ=26.2 (100m)

a) Depth of σ=27.2 (100m)

b) Streamlines on σ=26.2
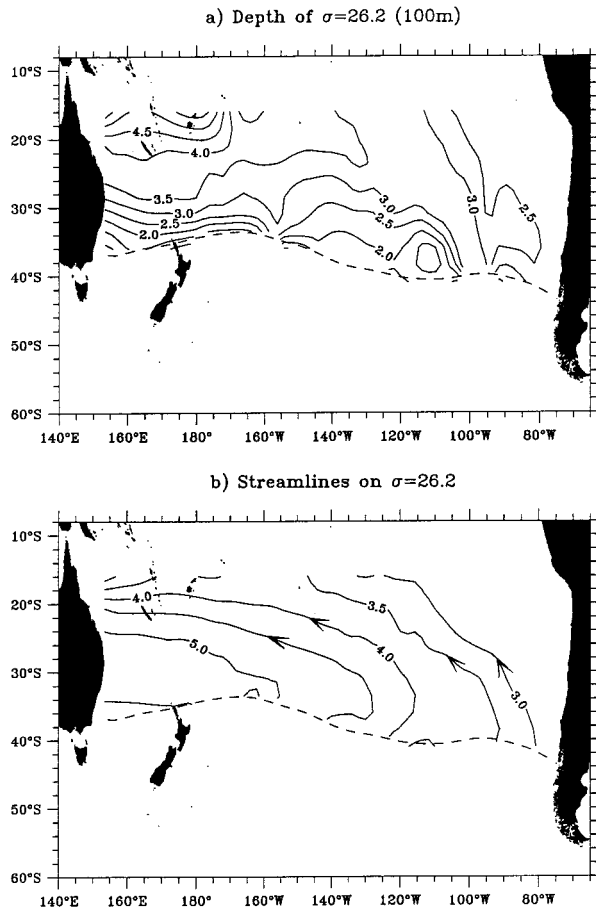
b) Streamline on σ=27.2

FIG. 11. (a) Depth and (b) streamlines of the $\sigma_\theta = 26.2$ isopycnal surface determined from the analytical model.
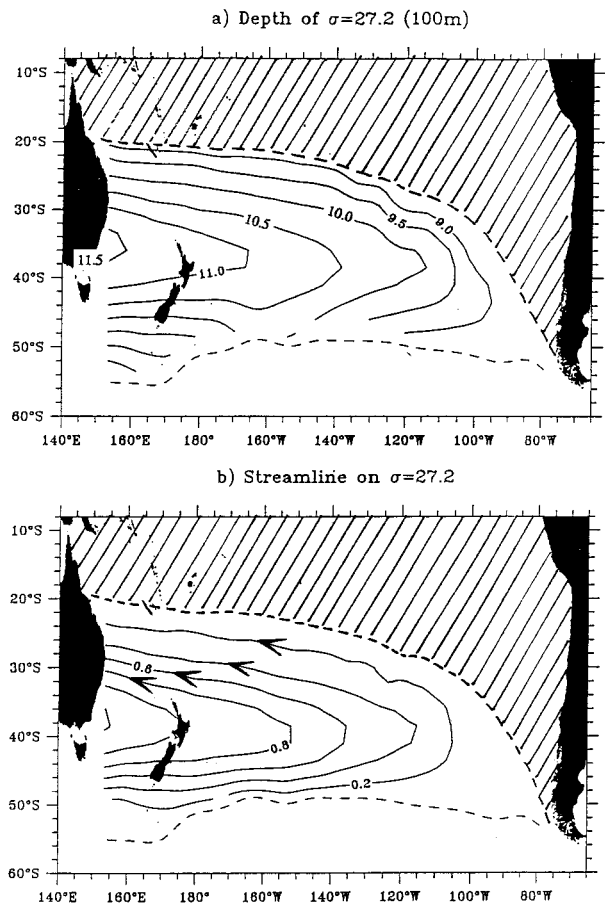
FIG. 12. (a) Depth and (b) streamlines of the $\sigma_\theta = 27.2$ isopycnal surface determined from the analytical model. The shaded areas indicate the shadow zone.

come to the conclusion that there is no subduction for isopycnal surfaces $\sigma_\theta \geq 26.6$. Thus the model seems to miss the formation of Antarctic Intermediate Water (AAIW).

However, if we separate obduction from subduction, there is indeed some AAIW formed in the models, as indicated by the thin solid line in Fig. 14c. Antarctic Intermediate Water (AAIW) is one of the major types of mode water in the Southern Ocean (McCartney 1977). One of its source regions is near the southern tip of South America. There is no reliable climatologic data on the mixed layer properties for this area. Rough estimates inferred from nearby hydrographic sections suggest that the winter mixed layer can reach about 800 m (McCartney 1977; M. S. McCartney 1996, personal communication; L. D. Talley 1996, personal communication). Using a numerical model, England et al. (1993) showed that winter convection reaches 1000-m depth and AAIW spreads horizontally around this level. Such deep convection is nearly smoothed out in the Levitus (1994) dataset. In fact, the maximum winter mixed layer depth in this location, calculated from the Levitus data, is no more than 450 m. As a result, the

Antarctic Intermediate Water formation near the southern tip of South America cannot be accurately simulated using the Levitus dataset.

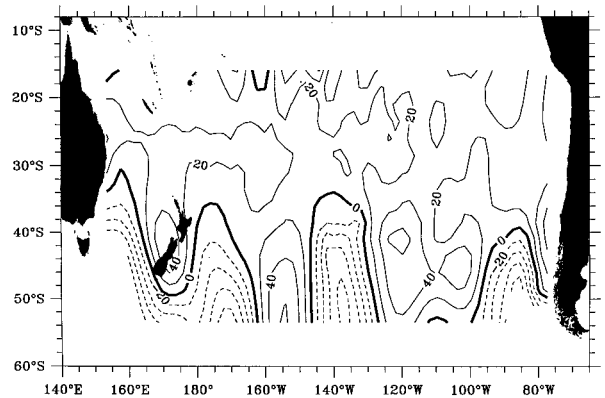On the other hand, the large disturbances appearing

FIG. 13. Subduction rate map calculated from the analytical model, in meters per year. Negative contours indicate obduction, that is, water from the thermocline flows upward/laterally into the mixed layer.
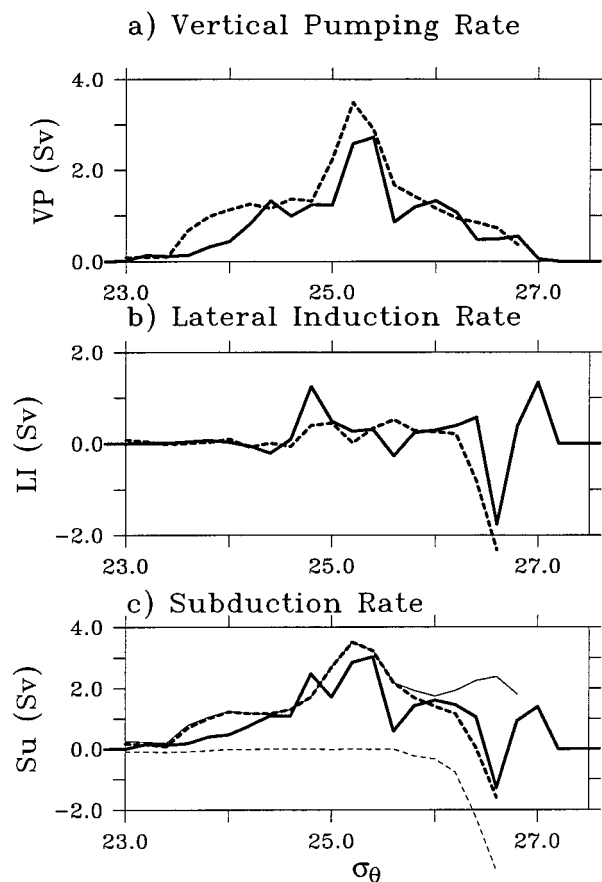
FIG. 14. Vertical pumping rate (a), lateral induction rate (b), and subduction rate (c) for each $0.2\sigma_\theta$ density interval, in Sverdrups. Solid lines are from the data analysis and dashed lines from the analytical model. Thin lines in (c) indicate the net subduction rate (solid thin line) and obduction rate (dashed thin line).
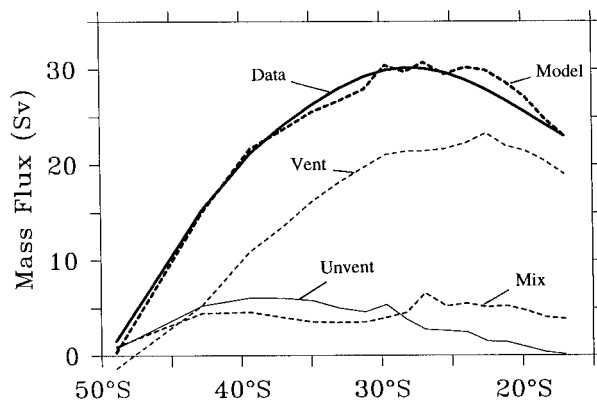

FIG. 15. Mass flux partition among the ventilated thermocline (Vent), the unventilated thermocline (Unvent), and the mixed layer (Mix) from the analytical model. The sum of these three components (Model) is indicated by the heavy dashed line on the top, compared with the barotropic mass flux calculated by integrating the Ekman pumping rate (Data) indicated by the heavy solid line.

in the winter mixed layer depth may not be entirely due to the paucity of the dataset. There is a major topographic feature, the East Pacific Rise near 120°W, that affects the Antarctic Circumpolar Current. As discussed by Gille (1995), downstream of the East Pacific Rise the jets associated with the ACC are less intense than they are upstream of the mid-Pacific ridge. However, the detailed dynamics of the interaction between the mixed layer and the ACC is left for further study.

The annual mean subduction rates estimated from the analytical and the diagnostic models show that there is only a moderate amount of subtropical mode water being formed annually in the South Pacific, Fig. 14. The water mass formation rate has a peak of 3 Sv in the density range of $\sigma_\theta = 25.3–25.5$; in other density ranges the water mass formation rate is well below 2 Sv. Subtropic mode water (STMW) has been studied in the North Atlantic (e.g., McCartney 1982) and in the North Pacific (e.g., Masuzawa 1969, 1972; Suga et al. 1989; Bingham 1992). In the South Pacific, STMW has received little attention because the STMW thermostad there is weak. A recent study by Roemmich and Cor-

nuelle (1992) identified the South Pacific STMW to be within the temperature range of 15°–19°C. The isopycnal surface of $\sigma_\theta = 25.5$ has a temperature around 16.5°C and lies in the core of the South Pacific STMW. According to Roemmich and Cornuelle, the lifetime of the South Pacific STMW is short so that, in spite of being locally formed as a mode water, it is not traceable to locations far from its formation zone.

The lack of strong subtropical mode water formation in the South Pacific (less than 3 Sv per $0.2\sigma_\theta$) is in sharp contrast to the high subtropical mode water formation rate (more than 4 Sv per $0.2\sigma_\theta$) in both the North Atlantic and the North Pacific (Qiu and Huang 1995).

Our analytical model also provides a three-dimensional view of the wind-driven gyre in the ocean interior. The Sverdrup mass flux is divided into three components, that is, the mass fluxes in the mixed layer, the ventilated thermocline, and the unventilated thermocline, Fig. 15. In previous studies, the term ventilation ratio was defined as the ratio beween the total mass flux in the ventilated thermocline and the total mass flux in the thermocline (e.g., Huang 1990; Huang and Russell 1994). Because the wind-driven circulation is essentially a three-dimensional feature, it may not be possible to represent the structure with some simple numbers, such as the ventilation ratio. In fact, if one defines the ventilation ratio as the ratio of mass flux in the ventilated thermocline to total mass flux in the thermocline, such a ventilation ratio apparently increases toward the equatorial boundary (Fig. 15). Mass flux in the unventilated thermocline declines toward the equator; meanwhile, the mass flux in the mixed layer remains almost constant. The small discrepancy between the barotropic Sverdrup flux and the sum of the baroclinic layers is due to the errors accumulated in the numerical calculation.

4. Summary

In this study we have applied both a diagnostic model and a simple analytical model to an analysis of the wind-driven circulation in the subtropical South Pacific. That these two approaches provided similar results is encouraging. For example, the total amount of ventilation and the contributions from vertical pumping and lateral induction in these two approaches are the same within the bounds of possible error.

The annual-mean subduction rate in the South Pacific is estimated in this study from both the analytical and diagnostic models. There are several sources of error in calculating the subduction rate. They include errors in the Ekman pumping rate, uncertainties in the mixed-layer density and background stratification patterns, and the assumption of the reference level. In the following, we evaluate some of the errors.

Neglect of the seasonal cycle in the mixed layer introduces errors. According to the definition, the subduction rate calculated in the analytical model is a local property, whereas the rate calculated by the diagnostic model involves averaging over 1-yr trajectories. By estimating subduction locally, the analytical model underestimates the annual subduction rate in the southern part of the subtropical basin but overestimates it in the northern part of the basin because the definition neglects changes in the Ekman pumping velocity along the 1-yr trajectories. Nevertheless, results from the two models are fairly similar. The major difference between the two approaches actually stems from the smoothing of the forcing fields used in the analytical model.

A major assumption of the Stommel demon is the shortness of the subduction period. Along the equatorial rim of the subtropical gyre, the base of the mixed layer is shallow and flat. The seasonal cycle is relatively weak and the subduction period may not be very short, so the subduction rate, especially the lateral induction term, calculated from the models may not be accurate.

Possible errors in the subduction rate can be roughly estimated as follows. The total amount of lateral induction is 3.5 Sv, and the difference between the late winter mixed layer depth maximum and minimum is $150 - 50 = 100$ m. Assume that the mixed layer depth maximum is increased to 175 m and the minimum mixed layer depth and the velocity at the base of the mixed layer remain approximately the same. Then the total amount of lateral induction in this case would increase to

$$3.5 \times \frac{175 - 50}{100} = 4.375 \text{ Sv}.$$

The total amount of vertical pumping at the base of the mixed layer will be slightly reduced; thus the total amount of subduction would increase less than 0.8 Sv.

There are two difficult issues associated with the accurate estimation of the subduction rate in the South Pacific. One is that there are few observations made in the Southern Ocean, so climatologies do not truly represent the time-mean ocean. The large variations in the winter mixed layer depth (Fig. 1a) may come from averaging over very limited observations. However, it is also possible that such large disturbances are some kind of permanent feature associated with bottom topography; this issue is left for further study.

The second issue is that both approaches used in this study assume the existence of a stagnant level somewhere above the ocean bottom. The diagnostic calculation is based on a reference level of 2000 m. As we noted in the previous section, the recent study of the hydrographic section along 32°S by Toole et al. (1994) indicates that in order to balance tracers it is necessary to put the reference level at the ocean bottom in the middle of the basin (120°–155°W). The ambiguity about the reference velocities may lead to the mass flux imbalance in the unventilated thermocline layer of our models.

A comparison between the ventilation in the North Atlantic and the North Pacific has been carried out by Qiu and Huang (1995). The differences between these two oceans include: First, the thermohaline circulation in the North Atlantic is quite strong, while that in the North Pacific is very weak with the upper ocean dominated by a shallow halocline. Second, the zero-Ekman-pumping line has a strong SW–NE tilt in the North Atlantic, while it is closer to a zonal line in the North Pacific. These differences give rise to different mixed layer properties and ventilation rates.

The present study provides an interesting comparison between the wind-driven circulation in the South Pacific and the Northern Hemisphere oceans (see Table 1). First, the mixed layer depths in most parts of the North and South Pacific are quite shallow and uniform. In the South Pacific, this is due to the lack of strong surface cooling (Oberhuber 1988), whereas in the North Pacific, it is due to the weak thermohaline circulation. As a result, contributions to the annual subduction rate due to lateral induction are quite small, about 9 Sv in the North Pacific and 3.5 Sv in the South Pacific. Relative to the total subduction rate, the lateral induction contributes about one-third in the North Pacific and one-sixth in the South Pacific. In contrast, the lateral induction term contributes one-half of the subduction rate in the North Atlantic.

Second, the wind-driven circulation in the South Pacific extends relatively deep; maximum depth is about 2.5 km near the northern edge of the Antarctic Circumpolar Current. In comparison, the wind-driven circulation in the North Pacific reaches only 1.4 km while in the North Atlantic it reaches 1.7 km (Huang 1990; Huang and Russell 1994). The relatively deep wind-driven circulation in the South Pacific is associated with the deep late winter mixed layer along the southern edge of the subtropical gyre.

Third, the mass flux in the unventilated thermocline is 19.8 Sv, about the same as in the North Atlantic (17.5

TABLE 1. Mass flux partition, in Sv (10^6 m³s⁻¹). Values of North Atlantic analytic are taken from Huang (1990) and those of North Pacific data analysis from Huang and Qiu (1994).

	North Atlantic analytic	North Pacific data analysis	South Pacific data analysis
A) Ekman pumping	16.2	28.8	25.3
B) Sverdrup transport	42	48	36
C) Ventilated thermocline:			
Vertical pumping	12.1	24.1	18.1
Lateral induction	12.7	9	3.5
Total subduction rate	24.8	31.1	21.6
D) Unventilated thermocline:			
1) Shallow unventilated	11	14	12.3
2) Deep unventilated	6.5	17.3	7.5
Total mass flux in unventilated thermocline	17.5	31.1	19.8

Sv), which is much smaller than that in the North Pacific (31.1 Sv). On the other hand, the total subduction rate in the South Pacific is only 21.6 Sv, much smaller than the 31.1 Sv in the North Pacific.

Fourth, the SE–NW tilted isopycnal outcropping lines in the eastern South Pacific give rise to an isopycnal slope reversal (i.e., shoaling of isopycnal surfaces westward), similar to the isopycnal outcropping line orientation and the associated isopycnal slope reversal that appear in the North Pacific subtropics (Hautala et al. 1994; Huang and Russell 1994).

The most serious problem in the South Pacific, particularly in the ACC region, is the lack of a reliable, large-scale climatological dataset. Results from both the diagnostic and analytical models provide a consistent picture for the subtropical mode water formation. On the other hand, neither approaches provides a reliable estimate for the formation and spreading of AAIW. Since our analytical model uses the $\sigma_\theta = 27.0$ isopycnal as the southern boundary, subduction of water heavier than 27.0 cannot be resolved in the model. In addition, the poor quality of the Levitus climatology in this area makes any diagnosis of water mass formation and movement vague. The results discussed in this study are our first attempt to reveal the structure of the wind-driven circulation there. Many uncertainties remain, as do many scientific questions, especially the formation of subantarctic mode water (SAMW) and AAIW, which greatly contribute to the deep circulation in the South Pacific. More observations are needed to improve our understanding of the Southern Hemisphere ocean.

REFERENCES

Bingham, F. M., 1992: Formation and spreading of subtropical mode water in the North Pacific. *J. Geophys. Res.,* **97,** 11 177–11 189.

Chelton, D. B., A. M. Mestas-Nunez, and M. H. Freilich, 1990: Global wind stress and Sverdrup circulation from the Seasat scatterometer. *J. Phys. Oceanogr.,* **20,** 1175–1205.

De Szoeke, R. A., 1987: On the wind-driven circulation of the South Pacific Ocean. *J. Phys. Oceanogr.,* **17,** 613–630.

England, M. H., J. S. Godfrey, A. C. Hirst, and M. Tomczak, 1993: The mechanism for Antarctic Intermediate Water renewal in a World Ocean model. *J. Phys. Oceanogr.,* **23,** 1553–1560.

Gille, S. T., 1995: Dynamics of the Antarctic Circumpolar Current: Evidence for topographic effects from altimeter data and numerical model output. Ph.D. thesis, Massachusetts Institute of Technology/Woods Hole Oceanographic Institute Joint Program, 198 pp.

Harrison, D. E., 1989: On climatological mean wind stress and wind stress curl fields over the World Ocean. *J. Climate,* **2,** 57–70.

Hautala, S. L., D. H. Roemmich, and W. J. Schmitz Jr., 1994: Is the North Pacific in Sverdrup balance along 24°N? *J. Geophys. Res.,* **99,** 16 041–16 052.

Haynes, P. H., 1985: Wind gyres in circumpolar oceans. *J. Phys. Oceanogr.,* **15,** 670–683.

Hellerman, S., and M. Rosenstein, 1983: Normal monthly wind stress over the World Ocean with error estimates. *J. Phys. Oceanogr.,* **13,** 1093–1104.

Huang, R. X., 1988: On boundary value problems of the ideal-fluid thermocline. *J. Phys. Oceanogr.,* **18,** 619–641.

——, 1990: On the three-dimensional structure of the wind-driven circulation in the North Atlantic. *Dyn. Atmos. Oceans,* **15,** 117–159.

——, and B. Qiu, 1994: Three-dimensional structure of the wind-driven circulation in the subtropical North Pacific. *J. Phys. Oceanogr.,* **24,** 1608–1622.

——, and S. Russell, 1994: Ventilation of the subtropical North Pacific. *J. Phys. Oceanogr.,* **24,** 2589–2605.

Iselin, C. O'D., 1939: The influence of vertical and lateral turbulence on the characteristics of the waters at mid-depths. *Trans. Amer. Geophys. Union,* **20,** 414–417.

Isemer, H. J., and L. Hasse, 1987: *The Bunker Climate Atlas of the North Atlantic Ocean.* Vol. 2. Springer-Verlag, 252 pp.

Jenkins, W. J., 1982: On the climate of a subtropical ocean gyre: Decade timescale variations in water mass renewal in the Sargasso Sea. *J. Mar. Res.,* **40** (Suppl.), 265–290.

——, 1987: ³H and ³He in the beta triangle: Observations of gyre ventilation and oxygen utilization rates. *J. Phys. Oceanogr.,* **17,** 763–783.

Large, W. G., and S. Pond, 1981: Open ocean momentum flux measurements in moderate to strong winds. *J. Phys. Oceanogr.,* **11,** 324–336.

Levitus, S., 1982: *Climatological Atlas of the World Ocean.* NOAA Prof. Paper No. 13, U.S. Dept. of Commerce, Washington, D.C., 173 pp.

——, 1994: *World Ocean Atlas 1994:* CD-ROM data set documentation. NODC Informal Report No. 13, National Oceanographic Data Center, Washington, D.C., 30 pp.

Luyten, J. R., J. Pedlosky, and H. Stommel, 1983: The ventilated thermocline. *J. Phys. Oceanogr.,* **13,** 292–309.

Marshall, J. C., A. J. G. Nurser, and R. G. Williams, 1993: Inferring the subduction rate and period over the North Atlantic. *J. Phys. Oceanogr.,* **23,** 1315–1329.

Masuzawa, J., 1969: Subtropical mode water. *Deep-Sea Res.,* **16,** 463–472.

——, 1972: Water characteristics of the North Pacific central region. *Kuroshio: Its Physical Aspects,* H. Stommel and K. Yoshida, Eds., University of Washington Press, 95–128.

McCartney, M. S., 1977: Subantarctic mode water. *A Voyage of Discovery: George Deacon 70th Anniversary Volume,* M. V. Angel, Ed., Suppl. to *Deep Sea Res.* Pergamon Press, 103–119.

——, 1982: The subtropical recirculation of mode waters. *J. Mar. Res.,* **40**(Suppl.), 427–464.

Oberhuber, J. M., 1988: *An Atlas Based on the ''COADS'' Data Set: The Budgets of Heat, Buoyancy, and Turbulent Kinetic Energy at the Surface of the Global Ocean.* Max-Planck-Institute for Meteorology, Rep. 15, 199 pp.

Qiu, B., and R. X. Huang, 1995: Ventilation of the North Atlantic and North Pacific: Subduction versus obduction. *J. Phys. Oceanogr.,* **25,** 2374–2390.

Reid, J. L., 1965: Intermediate waters of the Pacific Ocean. *Johns Hopkins Oceanogr. Stud.,* **2,** 85 pp.

——, 1986: On the total geostrophic circulation of the South Pacific Ocean: Flow patterns, tracers and transports. *Progress in Oceanography,* Vol. 16, Pergamon Press, 1–61.

Rhines, P. B., and W. R. Young, 1982a: Homogenization of potential vorticity in planetary gyres. *J. Fluid Mech.,* **122,** 347–367.

——, and ——, 1982b: A theory of the wind-driven circulation. I. Midocean gyres. *J. Mar. Res.,* **40**(Suppl.), 559–596.

Roemmich, D., and B. Cornuelle, 1992: The subtropical mode waters of the South Pacific Ocean. *J. Phys. Oceanogr.,* **22,** 1178–1187.

Sarmiento, J. L., 1983: A tritium box model of the North Atlantic thermocline. *J. Phys. Oceanogr.,* **13,** 1269–1274.

Stommel, H. M., 1979: Determination of water mass properties of water pumped down from the Ekman layer to the geostrophic flow below. *Proc. Natl. Acad. Sci., USA,* **76,** 3051–3055.

Suga, T., K. Hanawa, and Y. Toba, 1989: Subtropical mode water on the 137°E section. *J. Phys. Oceanogr.,* **19,** 1605–1618.

Talley, L. D., 1985: Ventilation of the subtropical North Pacific: The shallow salinity minimum. *J. Phys. Oceanogr.,* **15,** 633–649.

——, 1988: Potential vorticity distribution in the North Pacific. *J. Phys. Oceanogr.,* **18,** 89–106.

Toole, J. M., S. E. Wijffels, M. S. McCartney, B. A. Warren, H. L. Bryden, and J. A. Church, 1994: WOCE hydrographic section P6 across the subtropical South Pacific Ocean. *Proc. Pacific Basin Meeting,* Honolulu, Hawaii, W-SOPAC-06, 76.

Trenberth, K. E., W. G. Large, and J. G. Olson, 1990: The mean annual cycle in global ocean wind stress. *J. Phys. Oceanogr.,* **20,** 1742–1760.

Warren, B. A., 1973: Transpacific hydrographic sections at lats 43°S and 28°S: The SCORPIO Expedition—II. Deep water. *Deep-Sea Res.,* **20,** 9–38.

Welander, P., 1971: Some exact solutions to the equations describing an ideal-fluid thermocline. *J. Mar. Res.,* **29,** 60–68.

Williams, R. G., M. A. Spall, and J. C. Marshall, 1995: Does Stommel's mixed layer ''demon'' work? *J. Phys. Oceanogr.,* **25,** 3089–3102.

Woods, J. D., 1985: The physics of thermocline ventilation. *Coupled Ocean–Atmosphere Models,* (Chapter 34) J. C. J. Nihoul, Ed., Elsevier Science, 543–590.